PHYSICAL REVIEW E **81**, 020401(R) (2010)

Shear ordering in polymer photonic crystals

D. R. E. Snoswell,[1] A. Kontogeorgos,[1] J. J. Baumberg,[1,*] T. D. Lord,[2] M. R. Mackley,[2] P. Spahn,[3] and G. P. Hellmann[3]
[1]*Cavendish Laboratory, University of Cambridge, CB3 0HE Cambridge, United Kingdom*
[2]*Department of Chemical Engineering and Biotechnology, University of Cambridge, Cambridge, United Kingdom*
[3]*Deutsches Kunststoff-Institut (DKI), Schlossgartenstrasse 6, D-64289 Darmstadt, Germany*
(Received 5 June 2009; revised manuscript received 30 October 2009; published 12 February 2010)

Optical scattering spectra are recorded *in situ* on flowing colloidal polymeric nanocomposites which are sheared into photonic crystals at 150 °C using a high-pressure quartz-cell multipass rheometer. Broadband spectroscopy of the resonant Bragg scattering peak allows the direct observation of crystal formation and melting of monodisperse core-shell particles. A range of flow conditions of this solventless, highly viscous melt reveals four distinct regimes of crystal growth and decay which match a simple rheological model. Extraction of crystal thickness, order and lattice spacing are validated by one-dimensional electromagnetic simulations.

DOI: 10.1103/PhysRevE.81.020401 PACS number(s): 82.70.−y, 42.70.Qs, 47.50.−d, 81.16.Dn

Self-assembly of nanomaterials is key to their widespread utilization, however few practical examples currently exist. One recent success is polymer opals which are a unique form of colloidal photonic crystals that can now be made in large quantity through industrial processes including pressing, extrusion and rolling [1–4]. These rubberlike photonic crystals are durable and display reversible color changes when stretched or compressed, suggesting many practical applications [3]. Understanding the shear-ordering mechanism in these unique polymer opal systems is of significant scientific interest as they access new parameter regimes. Although studies have demonstrated shear ordering in colloidal systems for many years [5,6], the study of *highly viscous*, *solventless* assemblies of *soft-shelled* polymer opal spheres is new. Furthermore the *in situ* measurement of shear ordering in highly viscous ($\gg$100 Pas) systems of submicron spheres has not been previously attempted, requiring the development of experimental techniques capable of flowing highly viscous fluids while simultaneously allowing optical access.

Here, we develop a different technique to study crystal assembly and melting in highly viscous colloidal assemblies. Because we study the fundamental band gap of these colloidal crystals in the visible spectral region, dynamic diffraction measurements are not feasible (as the sub-200 nm wavelength UV light required does not propagate through these polymers). Hence we develop a technique recording the resonant scattering spectra in real time while the sample is sheared, in order to understand the formation of ordered crystals. In contrast to previous studies with Péclet numbers $\mathrm{Pe} \ll 1$ [7–13], our work explores the high viscosity regime $\mathrm{Pe} > 1$ with a colloidal system that contains no continuous liquid phase since the 'fluid' consists of soft shells anchored to each individual particle core. Although we find evidence for crystal phases [11], shear-induced changes in order [12], and rheological transitions [13] seen in other studies of oscillatory flows, the lack of significant thermal diffusion in our study is unique, resulting in rapid crystal growth dependant on accumulating strain, up to a yield point which is independent of shear rate.

The polymer opal core-shell particles consist of rigid, highly crosslinked (10 wt% butanediol diacrylate) polystyrene cores of size 167 nm encapsulated in a poly-methylmethacrylate (PMMA) interlayer (thickness 9 nm) to which a soft polyethylene acrylate (PEA) shell is chemically grafted to give an outer particle size of 246 ± 16 nm [2]. We have previously demonstrated that lightly doping such colloidal particles with scattering nanoparticles dramatically increases the resonant Bragg scattering of light [1], and hence these polymer particles were thoroughly mixed together with 0.05 wt % sub-50 nm carbon black (Special Black 4, Evonik) in a twin screw compounder for 15 min at 150 °C.

The large viscosity of these samples prevents the use of conventional opto-rheological techniques such as oscillating shear plates as these cannot exert the high pressures and stresses required to induce flow, hence we use a customized optically accessible multipass rheometer (MPR) [14]. This polymer opal blend is loaded into the MPR which is preheated to 150 °C [Fig. 1(a)]. After carefully expelling the air from the sample cavity in the MPR, optical experiments are performed with preprogrammed piston movements [Fig. 1(b)]. Computer control of the piston position allows precise control of sample flow conditions and piston speeds as slow as 1 μm/s can be achieved.

Light from an incandescent halogen source is focused on the inside face of the quartz window using a 75 mm focal length lens resulting in an illuminated spot diameter of 1 mm, incident at 15°. Backscattered light ($\theta_{out}=-15°$) is collected through the same lens and relayed to a spectrometer via a pellicle beamsplitter. Spectra are normalized with respect to a Lambertian white diffuser. Repeated spectra with a 40 ms integration time are collected simultaneously with piston position and pressures (read directly from MPR sensors) allowing precise synchronization of the data.

In this Rapid Communication we concentrate on the flow and ordering obtained with periodically driven sinusoidal piston movements (in which both pistons move in the same direction) allowing the effects of shear strain to be tracked [Figs. 1(b) and 1(c)]. The pressure difference generated across the cavity causes the viscous polymer opal to flow back and forth. Large changes in the recorded spectra are observed just after the piston motion changes direction [Figs. 1(b) and 1(c) P and Q]. A range of sinusoidal piston movements with different frequency (0.01, 0.02, 0.03 Hz) and

*jjb12@cam.ac.uk

 ©2010 The American Physical Society

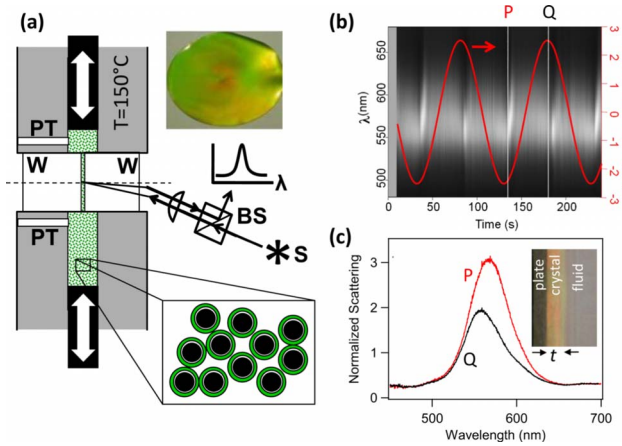

FIG. 1. (Color online) (a) Setup: hydraulic pistons (diameter 10 mm) force core-shell particles through rectangular cavity ($10\times10\times1.5$ mm) formed between quartz windows (w) within a temperature-controlled jacket. Light source (s) is focused onto the inside face of the window at 15° incidence, and backscattered light collected via a beamsplitter (BS) to a spectrometer. Pressure is measured either side of the cavity (PT). Inset: 10 cm diameter polymer opal film. (b) Time-resolved spectra (left λ scale, white is strong scattering) with piston motion superimposed (red, right axis). (c) Spectra from cuts P and Q in (b). Inset: Dark-field microscope image of cross section of compression-sheared polymer opal, crystalline top layer thickness $t=50$ μm appears colored.

amplitude (2.5 and 1.0 mm) are explored resulting in maximum piston velocities between 7 and 500 μm/s. For all of these piston motions the spectral changes occur approximately at the same piston *position*, suggesting that *shear strains* rather than *shear rates* are the crucial control parameter. For each sinusoidal piston movement, systematic spectral differences between top and bottom piston turnarounds are always observed. These direction-dependent spectral differences are likely to be due to slight differences in the flow geometries around the entry to the narrow flow channel, and are not the focus of this investigation. Critically however, the repeatability of spectral changes occurring after each turnaround of the same type is very high.

By comparing data from the same experimental run but at exactly one time period apart, the repeatability of the spectral changes is clearly shown [Fig. 2(a), black and green points]. The spectral scattering data are analyzed extracting the peak height, center wavelength and linewidth as a function of time [Fig. 2(a)]. The highly evident changes in the resonant Bragg scattering peak are due to structural rearrangements within the opal and can be divided into four distinct time regions corresponding to four structuring processes (Fig. 2, A–D). As the scattering peak becomes transiently stronger, it first blueshifts and narrows, then redshifts and broadens. These characteristic features observed are present for all piston motions. This is the first time the process of crystallization in a solventless colloidal system has been captured in detail through resonant Bragg scattering spectroscopy (since it demands such small sub-λ sphere sizes) and a wealth of complexity is revealed.

To understand the origin of these effects we develop a simple one-dimensional (1D) multilayer model, restricted to

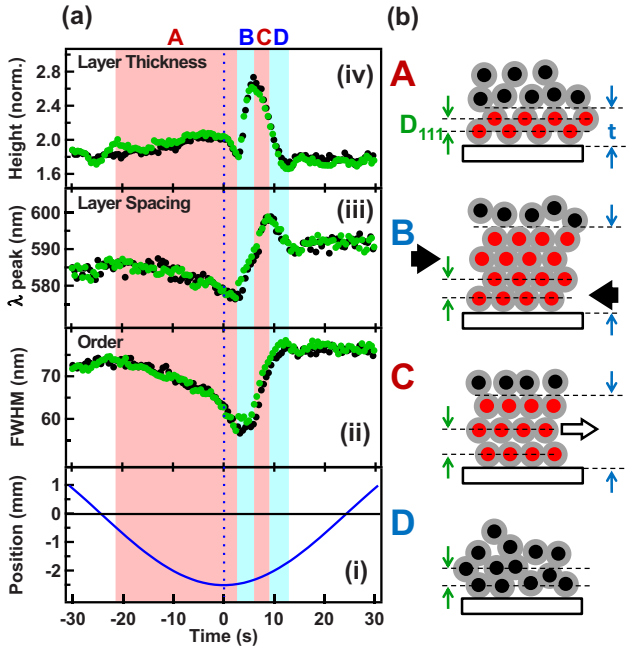

FIG. 2. (Color online) (a) Flow-induced spectral changes with sinusoidal piston motion (i) extracted as: (ii) scattering peak width, (iii) peak wavelength, and (iv) peak height. Two data sets (black, green) taken from the same run one time period apart confirm reproducibility. Four characteristic particle reordering regimes are labeled A-D and depicted in (b), with red particles crystallized and black particles in disordered sheet flow. Layer separation is D_{111}, thickness of crystal layer is t, black arrows in B signify shear and compression, and the white arrow in C shows relative movement of adjacent planes.

the (111) planes giving rise to the experimental spectra, and incorporating disorder based on simple transfer-matrix calculations averaged over different structural realizations [15]. Full three-dimensional electromagnetic simulations in these low refractive index contrast ($\Delta n=0.1$) opal systems are computationally prohibitive due to the long optical penetration lengths, but support our interpretation of the 1D model. We use a quarter-wavelength-stack distributed feedback reflector with $\Delta n=0.1$ and $\bar{n}=1.55$ in which each interface is randomly displaced by a Gaussian-distributed disorder parameter, $\bar{\delta}$. As the disorder increases, the typical rectangular stop band becomes weaker, broadened and Lorentzian [Fig. 3(a)]. These simulations are averaged over 100 realizations of specific disorder profiles to reflect the measurements averaging over locally different sample regions. Adding further layers is confirmed not to affect the results, in accordance with the expected optical penetration. An important result not previously noted is the emergence of Lorentzian spectra with broad spectral wings (that do not decay exponentially). Considering the Fourier Transform of these spectra suggests disordered modes are spatially localized within this quasiperiodic structure [16]. We observe that a decrease in the order within the structure increases the peak width [Fig. 3(a)] in accordance with experimental observations [17], while an increase in the number of crystalline layers causes the peak height to increase [Fig. 3(b)]. While increasing disorder decreases the peak height, the peak width is unaffected by the

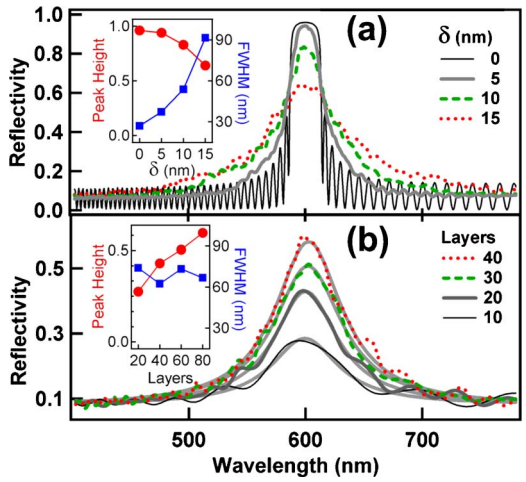

FIG. 3. (Color online) Simulated optical reflectivity of 1D photonic crystals of $\Delta n=0.1$ with average layer thickness 200 nm incorporating (a) increasing disorder, $\bar{\delta}=0,5,10,15$ nm, for 80 double layers, and (b) increasing numbers of layers for $\bar{\delta}=15$ nm (Lorentzian fits included). Spectra are averages of 100 separate configuration simulations. Insets summarize changes in line width (squares) and peak reflectivity (circles).

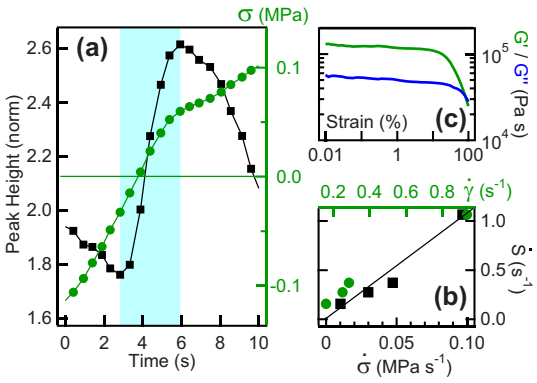

FIG. 4. (Color online) (a) Shear stress (circles) and scattering peak height (squares) vs time after piston turnaround. Crystal-growth region shaded (region B). (b) Crystal growth rate $\dot{S}=d/dt$ (peak height) versus rate of applied shear stress $\dot{\sigma}$ and maximum shear rate in region B for different sinusoidal piston motions. (c) Rheology obtained with torsionally oscillating parallel disks (25 mm diameter) at 150° showing, storage G' and loss G'' modulus for strain sweep at $\omega=10$ rad s^{-1}.

number of layers. In summary, this model confirms that peak height tracks the number of layers, peak width tracks the disorder in the crystal and peak wavelength is proportional to the average layer separation. Using this interpretive framework allows analysis of the structuring mechanisms observed in Fig. 2(a).

In region A, the piston slows as it approaches the piston turnaround point (vertical dashed line). During this region the peak height slightly increases while the peak width and wavelength decrease. This corresponds to mechanism A where an ordered crystalline layer grows out from the quartz window toward the interior of the cavity. The wall templates and nucleates the first crystal plane [11,18] similar to studies observing crystallization at the cessation of shear [19,20]. Video microscopy of crystal formation in region A reveals that crystalline polymer opal domains are stationary at the wall surface compared with noncrystalline regions [Fig. 1(c) inset]. A 10 nm (1.7%) blueshift in the wavelength indicates that the effective layer separation ($\simeq$190 nm) decreases proportionally by 3 nm, implying that particles in adjacent layers become interleaved (since this thickness is less than the particle diameter). Although shear-induced crystallization in monodisperse colloidal systems is frequently observed [20–22], observations of changes in layer separation are not frequently reported.

Just *after* the piston turnaround (region B) the growth rate of the crystalline layer thickness increases dramatically as indicated by the steep increase in peak height, while the wavelength redshifts without changing the peak width. Crystal formation can cause a drop in viscosity when layers of particles slide past one another [11,13,21,22]; however, our solventless system of soft spheres resists particle sliding below a threshold shear stress. In low viscosity systems where the particle sliding motions are lubricated by a fluid, the threshold shear stress of the crystal phase may be very low allowing layer sliding, even while crystal growth is occurring [21,22]. However in our solventless system, a stationary crystal grows until the yield stress of the crystal is exceeded and layer sliding commences (region C). Shear stress at the wall can be simply calculated from the pressure drop, the cross section and the surface area. Rapid crystal growth arises when the absolute shear stress, $|\sigma|<0.06$ MPa [Fig. 4(a)], with all data sets (varying piston amplitude and frequency) revealing similar thresholds (0.02–0.09 MPa). This threshold is the yield stress of the crystal structure. Shear stress crosses zero at slightly later times after piston turnaround because of the compressibility of the polymer opal (1% volume decrease per 8.8 MPa).

During this period of rapid crystal growth the particles must rearrange from the glassy to crystal state by a cage breaking mechanism which engages over a certain shear threshold [11,13]. In our system, thermal diffusion which promotes crystal melting is negligible, thereby maximizing the crystal-growth rate and lowering the strain threshold to induce crystallization [13]. In our data we could not confidently identify a lower shear limit for cage breaking due to measurement resolution, with crystal growth even occurring at slightly negative shear stress in some cases. Crystal growth rates, $\dot{S}$, in region B were proportional to the shear rate and rate of shear stress [over all data sets, Fig. 4(b)], consistent with a cumulative shear-ordering process of a predominately elastic material [Fig. 4(c)] during "creeping flow" [23,24].

Assuming a parabolic flow profile, estimated strains at the onset of crystal melting (yield point, Region B/C transition) were essentially constant within error, ranging from 60% to 100% for all data sets, in agreement with the yield points determined by rheology [Fig. 4(c)] and previous work [13]. Constant crystal yield strains showed *no correlation* to the shear rates at the yield point which varied from 0.16 to 0.94 s^{-1}, consistent with the absence of thermal diffusion.

During crystal growth we observe a redshift of the peak wavelength, caused by simultaneous in-plane compression [Fig. 2(b), black arrows], separating adjacent layers and reducing the interleaving of spheres. Self-diffusion of particles is known to increase along specific oriented directions within sheared colloids of high Péclet numbers [9] aiding the crystal growth. High Péclet numbers generally enhance shear ordering [25] and here $\mathrm{Pe} \approx 20\,000$ which is 100 times greater than studied in other colloidal systems.

Region C is marked by a sudden decrease in peak height, caused by "shear melting" of the layers furthest away from the wall [26–29], thereby decreasing the total number of ordered layers. Above the crystal yield stress, layers of close-packed spheres flow past one another [11,13,21]. At the same time, stresses involved in the disruption of the outer layers propagate to the ordered layers near the wall causing a decrease in order and a corresponding rapid increase in peak width. At the onset of shear melting there is a corresponding reduction in the rate of shear stress [Fig. 4(a)] similar to previous observations [13,30]. Further separation of adjacent layers is indicated by redshifts in the peak wavelength, corresponding to slippage between planes [Fig. 2(b), white arrow]. This overall 20 nm (3.5%) redshift in regions B,C implies that the layers move on average 3.5% further apart before melting initiates. Shear-induced phase transitions from crystal to sliding crystal planes have been observed previously [11,13,30]. More recent studies considering the flow-induced movement of spheres in a close-packed lattice show they follow a zig-zag path along slip directions over the saddle of spheres in neighboring layers [10,12]. In this model, the spheres lift 6% above their close-packed layer spacing, producing a time-averaged increase of the layer spacing around half this value, and thus in good agreement with the experiment. In this regime, because the PS cores remain incompressible, the shells take up large strains exceeding 20%.

Finally, the peak wavelength abruptly blueshifts in region D returning to the disordered glassy state of the polymer opal, where most of the crystal layers built in region B have been melted. Nevertheless the monodispersity of the particle sizes imparts residual disordered layer structure that gives the remnant resonant scattering spectra. Through this full cycle, the 3.5% maximum change in layer spacings corresponds to disorder $\bar{\delta} \simeq 5$ nm producing estimated FWHM linewidths of 50 nm [Fig. 3(a)] in good agreement with those experimentally measured.

In summary, the optical properties of solventless polymer opal samples have been studied *in situ* as flow conditions are precisely controlled. Repeatable systematic evolution of the optical scattering spectra can be divided into four distinct regimes, controlled by the net elastic shear strain. At extreme viscosities with Pèclet numbers 100 times those in previous colloidal work, thermal diffusion is negligible resulting in rapid crystal growth and an immeasurably low threshold at which the glass to crystal transition occurs. Crystal growth occurs in the elastic regime via a *creeping sphere flow* mechanism while *shear-induced layer flow* is shown to destroy the sphere ordering. This produces sharply defined layers of ordered opal nucleated from the walls, capped by layers of flowing disordered spheres. We find that optical modeling of such structured nanomaterials using low-Δn contrast multilayers incorporating few % disorder, gives good agreement with experiment, providing estimates of crystalline region thickness, order and layer spacing. These measurements of solventless photonic crystal yield stress and shear-ordering growth rate provide important data in a regime where thermal motion is negligible while also aiding industrial manufacture of structural color materials.

This work was supported by UK EPSRC-GB Grants No. EP/C511786/1, No. EP/G060649/1, and No. EP/E040241.

[1] O. L. Pursiainen *et al.*, Opt. Express **15**, 9553 (2007).
[2] T. Ruhl *et al.*, Polymer **44**, 7625 (2003).
[3] B. Viel *et al.*, Chem. Mater. **19**, 5673 (2007).
[4] O. L. Pursiainen *et al.*, Adv. Mater. **20**, 1484 (2008).
[5] N. A. Clark and B. J. Ackerson, Phys. Rev. Lett. **44**, 1005 (1980).
[6] H. J. M. Hanley *et al.*, J. Phys. Chem. **79**, 4448 (1983).
[7] R. Besseling *et al.*, Phys. Rev. Lett. **99**, 028301 (2007).
[8] I. Cohen *et al.*, Phys. Rev. Lett. **97**, 215502 (2006).
[9] V. Breedveld *et al.*, J. Chem. Phys. **116**, 10529 (2002).
[10] D. Derks *et al.*, Soft Matter **5**, 1060 (2009).
[11] B. J. Ackerson, J. Rheol. **34**, 553 (1990).
[12] M. D. Haw *et al.*, Phys. Rev. E **57**, 6859 (1998).
[13] N. Koumakis *et al.*, Soft Matter **4**, 2008 (2008).
[14] M. R. Mackley *et al.*, J. Rheol. **39**, 1293 (1995).
[15] A. V. Kavokin *et al.*, *Microcavities* (Oxford University Press, Oxford, 2007).
[16] H. Cao *et al.*, Phys. Rev. Lett. **84**, 5584 (2000).
[17] R. Rengarajan *et al.*, Phys. Rev. E **71**, 016615 (2005).
[18] J. P. Hoogenboom *et al.*, J. Chem. Phys. **117**, 11320 (2002).
[19] R. J. Butera *et al.*, Phys. Rev. Lett. **77**, 2117 (1996).
[20] P. Panine *et al.*, Phys. Rev. E **66**, 022401 (2002).
[21] Y. L. Wu *et al.*, Proc. Natl. Acad. Sci. U.S.A. **106**, 10564 (2009).
[22] J. M. McMullan and N. J. Wagner, J. Rheol. **53**, 575 (2009).
[23] K. N. Pham *et al.*, J. Rheol. **52**, 649 (2008).
[24] A. Le Grand and G. Petekidis, Rheol. Acta **47**, 579 (2008).
[25] J. Vermant and M. J. Solomon, J. Phys.: Condens. Matter **17**, R187 (2005).
[26] T. Sawada *et al.*, Jpn. J. Appl. Phys., Part 2 **40**, L1226 (2001).
[27] A. Imhof *et al.*, Langmuir **10**, 3477 (1994).
[28] R. L. Hoffman, J. Rheol. **16**, 155 (1972).
[29] P. Holmqvist *et al.*, Langmuir **21**, 10976 (2005).
[30] L. B. Chen *et al.*, J. Rheol. **38**, 193 (1994).